processes

MDPI

Article

Markov-Chain-Based Statistic Model for Predicting Particle Movement in Circulating Fluidized Bed Risers

Yaming Zhuang

School of Mechanical and Electrical Engineering, Suqian University, Suqian 223800, China; ymzhuang@squ.edu.cn

Abstract: To increase the calculation speed of the computational fluid dynamics (CFD)-based simulation for the gas–solid flow in fluidized beds, a Markov chain model (MCM) was developed to simulate the particle movement in a two-dimensional (2D) circulating fluidized bed (CFB) riser. As a statistic model, the MCM takes the results obtained from a CFD–discrete element method (DEM) as samples for calculating transition probability matrixes of particle movement. The transition probability matrixes can be directly used to describe the macroscopic regularities of particle movement and further used to simulate the particle motion combined with the Monte Carlo method. Particle distribution snapshots, residence time distribution (RTD), and mixing obtained from both MCM and CFD-DEM are compared. The results indicate that the MCM offers a computational speed that is approximately 100 times faster than that of the CFD-DEM. The discrepancy in the mean particle residence time, as computed by the two models, is under 2%. Furthermore, the MCM provides an accurate depiction of time-averaged particle motion. In sum, the MCM can well describe the time-averaged particle mixing compared to the CFD-DEM.

Keywords: Markov chain; statistic model; fluidized bed; CFD-DEM

check for updates

Academic Editor: Alberto Di Renzo

Received: 21 January 2025
Revised: 10 February 2025
Accepted: 19 February 2025
Published: 21 February 2025

Citation: Zhuang, Y. Markov-Chain-Based Statistic Model for Predicting Particle Movement in Circulating Fluidized Bed Risers. *Processes* **2025**, *13*, 614. https://doi.org/10.3390/pr13030614

Copyright: © 2025 by the author. Licensee MDPI, Basel, Switzerland. This article is an open access article distributed under the terms and conditions of the Creative Commons Attribution (CC BY) license (https://creativecommons.org/licenses/by/4.0/).

1. Introduction

The circulating fluidized bed (CFB) is widely used in a variety of processes, such as power plants and chemical and pharmaceutical industries due to its excellent gas–solid interactions and the ability to reduce pollutant emissions [1,2]. In terms of computer technology and computing algorithm advances, numerical simulation has emerged as a prevalent and efficient approach for studying complex gas–solid two-phase flow in fluidized beds, which is instructive for an improvement in the actual industrial process and substantially reduces the experimental cost. A two-fluid model (TFM) [3–5] under the Eulerian–Eulerian framework and computational fluid dynamics–discrete element method (CFD-DEM) [6–8] under the Eulerian–Lagrangian framework are two of the most used modeling methods in the simulation of gas–solid fluidized beds. In particular, the CFD-DEM takes the interaction between particles into account, which can provide a relatively accurate and detailed particle moment [9–12]. However, the high computational load and long computing time restrict the practical application of this model as it needs to solve the fundamental equations of fluid and particle dynamics.

The Markov chain model (MCM) has been proven to be a highly productive and reliable approach for modeling particle processes within granular systems, which calculates particle motion through the transition probability matrix and Monte Carlo method without solving the complicated dynamic formulae [13–15]. Berthiauxa et al. [16,17] introduced some applications of the Markov chain theory to simulate different processes of particle

technology, such as grinding, classification, mixing, and agglomeration. The examples confirmed that the Markov chain theory was a universal mathematical tool and it only contained few mathematical operations, which could be easily performed by using contemporary software. As a typical granular system, the rotating drum was simulated by Doucet et al. [18] using the Markov chain theory. They defined the Markov states of the rotating drum by the divisional physical cells. In this way, the specific particle movement could be obtained by the MCM. The calculation of the transition probability matrix was based on directly taking the preliminary DEM simulated results as statistic samples, since the DEM was able to give detailed particle movement. The simulated results showed that the MCM gave a good estimate of the particle mixing in the rotating drum system. Ponomarev et al. [19,20] established a 2D model of the flow and mixing of particulate solids for an alternately revolving static mixer based on the Markov chain theory. The particle transition probability between each two mixing elements was calculated according to the physical geometry. Effects of the initial material loading and the transition probability values on the mixing kinetics were investigated. In addition, a comparison of the simulated results with the published experimental data gave a good validation of the viability of the MCM.

However, when considering fluidized beds, the interaction between the solid phase and the gas phase is much stronger and more complicated than that in both the rotating drum and the static mixer. Regardless, there has been some research about the application of the MCM in fluidized beds. Gottschalk et al. [21] introduced a multiphase stochastic model for vertical particle transport in bubbling fluidized beds based on the Markov chain theory. The finite velocity of fluidization bubbles and the extra particle transport due to gulf streaming were considered in the description of Markov chain states. Results from the multiphase stochastic model agreed well with the experimental data. But neither the horizontal particle transport nor the detailed particle moment could be obtained from the simulation of this stochastic model. Catak et al. [22,23] introduced a Markov chain simulation for the fluidized bed granulation. However, the Markov chain method was only used to model and analyze the particle size enlargement process, but was not involved with the particle fluidization. Mizonov et al. [24–26] proposed a one-dimensional mathematical model of particulate solid fluidization based on the theory of Markov chains. Particle convection between two different cells of the chain and the particle diffusion over the bed height were taken into consideration to calculate the transition probabilities. The model successfully described and predicted the macroscopic particulate phase distribution over the bed height in the batch process, and the particle residence time distribution (RTD) was verified experimentally. Harris et al. [27] presented two stochastic mathematical models to simulate the RTD of solids in the riser of a CFB using a Markov chain. One of them was a core-annulus solid interchange model, and the other was a four-zone model that was derived from the fast fluidized bed hydrodynamic profile. The transfer probabilities were calculated according to the local particle mass flow rates between each two states, and with both the discrete time and the continuous time versions presented. The particle RTDs simulated by the stochastic models were in good agreement with the experimental data from a few authors. Nevertheless, the MCMs mentioned above can only simulate the macro movement of many particles, but cannot provide as detailed particle movement in the fluidized beds as that predicted by the CFD-DEM simulation. However, it is hard to find more references that compare MCM results with experimental fluidized bed data which focus on the detailed particle movement. Therefore, there remains a significant distance to bridge the gap between integrating the MCM with the chemical reactions and mass and heat transfers.

In this paper, an MCM is introduced to simulate detailed particle movement in a 2D CFB riser, which is carried out through discretizing the CFB riser into physical cells as Markov states. As the CFD-DEM can provide a relatively accurate and detailed particle moment in fluidized beds, the previous CFD-DEM results can act as appropriate statistical samples for the MCM, and the subsequent CFD-DEM simulation is used to verify the calculated results of the MCM. In addition, as the MCM belongs to the statistical category, the informative sample data provided by CFD-DEM is beneficial for the improvement and further expansion. Furthermore, statistical models have strong sample adaptability. The MCM established based on CFD-DEM simulation results can easily replace samples with experimental data in the future.

2. Models and Methods

2.1. Research Object and CFD-DEM

An infinite 2D CFB riser is simulated in this research, and MATLAB R2022a developed by MathWorks, Inc. (1 Apple Hill Drive, Natick, MA 01760-2098, USA) and Visual Studio 2022 developed by Microsoft Corporation (One Microsoft Way, Redmond, WA 98052, USA) are used. The gas and particles exiting the riser are instantaneously introduced into the inlet, maintaining the same velocity and lateral positions. Details of the CFB riser and CFD-DEM model are listed in Table 1.

Table 1. Details of the CFB riser and CFD-DEM.

Bed size	0.09×0.95 m^2
Particle density	2600 kg/m^3
Particle diameter	0.001 m
Particle number	27,000
Inlet air velocity	3 m/s, 4 m/s, 6 m/s, 8 m/s
Minimum fluidization velocity	0.44 m/s
Cells number of CFD	9×95
Cells number of DEM	30×351
Time step of CFD	5×10^{-5} s
Time step of DEM	5×10^{-6} s
Normal stiffness	10,000 N/m
Tangential stiffness	2857 N/m
Normal restitution coefficient	0.97
Tangential restitution coefficient	0.33
Frictional coefficient	0.1

CFD-DEM can simulate detailed particle motion in the CFB riser based on the fundamental equations of fluid and particle dynamics, which is convenient for statistical calculation. Using CFD-DEM results as samples for the MCM is an efficient and optimal approach [18,28,29]. In the CFD-DEM model, the basic drag model [30] and liner spring-dashpot model [11] are contained. All particle collisions are considered in the CFD-DEM simulation. The CFD-DEM simulation lasts 20 s and the MCM takes the results from 10 s to 15 s as samples to calculate the statistical laws, as fluidization is fully developed in this period. The calculation of MCM lasts 5 s based on the statistical laws. The results calculated by MCM are compared with those from CFD-DEM during the same period (15 s–20 s).

2.2. Markov Chain Model

In terms of mathematical form, a stochastic process can usually be represented as a collection of random variables. The set of all possible values that a stochastic process can take is called the state space of the process. A Markov chain represents a specific type of stochastic process which satisfies the Markov property. This property states that the

conditional probability distribution for a system's future state is solely dependent on the current state [16]. At each step of a Markov chain, the system can transition from one state to another or remain in the current state based on a probability distribution. This change in state is called a transition, and the probabilities associated with different state changes are known as transition probabilities. In this paper, a discrete-time Markov chain is employed, where transitions between states in a state space occur based on the probability distribution of the subsequent state. The distribution of probabilities is solely determined by the present state, unaffected by the previous sequence of events. Although strictly verifying the Markov property in fluidized beds is extremely challenging, several applications and discussions have persuasively demonstrated the applicability of MCM methods for fluidized beds [21].

The fluidized bed can be divided into grids based on physical space to define the Markov state space for particles. For any particle in a fluidized bed, its grid information represents a state of its random motion process within the fluidized bed. This way, a statistical model that can simulate relatively detailed particle motion processes can be established, and the model has the foundation for further coupling chemical reactions, heat transfer, and mass transfer in subsequent steps. In this research, a 2D CFB riser is divided into m equal sections along its width and n equal sections along its height. The physical cells represent the spatial states of the MCM, as shown in Figure 1. The space state information of a particle at a certain time t_c can be described by a state vector $\boldsymbol{S}(t_c)$, as follows:

$$\boldsymbol{S}(t_c) = [s_1(t_c), s_2(t_c), \ldots, s_{n \cdot m}(t_c)],\ sum\{\boldsymbol{S}(t_c)\} = 1 \quad (1)$$

$\boldsymbol{s}_{(n-1)\cdot m+1}$	$\boldsymbol{s}_{(n-1)\cdot m+2}$	⋯	$\boldsymbol{s}_{n\cdot m}$
⋮	⋮	⋮	⋮
$\boldsymbol{s}_{m+1}$	$\boldsymbol{s}_{m+2}$	⋯	$\boldsymbol{s}_{2\cdot m}$
$\boldsymbol{s}_1$	$\boldsymbol{s}_2$	⋯	$\boldsymbol{s}_m$

Figure 1. Discretized CFB riser with $n \cdot m$ cells (space states).

If a particle is in the nth grid at the current moment, then the value of the nth element $s_n(t_c)$ of the state vector $\boldsymbol{S}(t_c)$ is marked as 1, while other elements are marked as 0. This state is referred to as the Markov state $\boldsymbol{S}(t_c)$ of the particle. At the beginning, the cell where the particle is located represents its MCM state, and the corresponding component of $\boldsymbol{S}(t_c)$ is assigned the value 1, while other elements are assigned a value of 0.

Figure 2 gives a diagram of the transitions of the Markov chain states, assuming that there are $N_i(t_c)$ particles in the state s_i at the time t_c, and there are $N_{ij}(t_c)$ particles

moving from s_i to s_j at the next moment t_{c+1}. The transition probability $p_{ij}(t_c)$ describes the probability that particles move from s_i to s_j between the moment t_c, and t_{c+1} can be calculated as in Equation (2).

$$p_{ij}(t_c) = \begin{cases} \frac{N_{ij}(t_c)}{N_i(t_c)}, & N_i(t_c) \neq 0 \\ 0, & N_i(t_c) = 0 \end{cases} \tag{2}$$

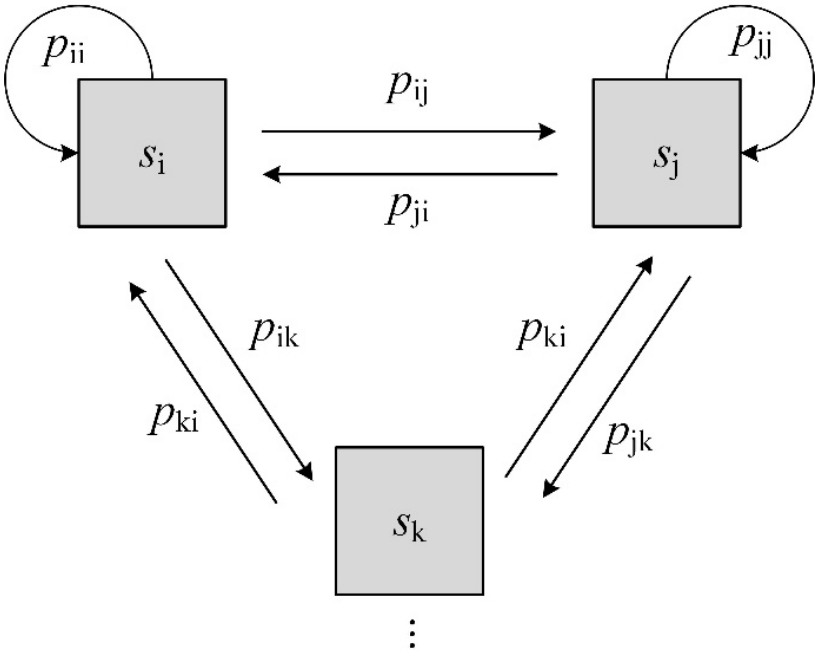


Figure 2. Diagram of the transitions of Markov chain states.

Transition probabilities between any other two states at any time moment can be calculated by the same method, which form a matrix $\boldsymbol{P}'(t_c)$ of the transition probabilities at this time. The mean of all transition probability matrixes at all moments is the final transition probability matrix $\boldsymbol{P}$ for the MCM. All information of the particles used in the calculation of the transition probabilities is obtained from the CFD-DEM results. Matrixes $\boldsymbol{P}'(t_c)$ and $\boldsymbol{P}$ are shown as Equations (3) and (4).

$$\boldsymbol{P}'(t_c) = \begin{bmatrix} p_{11}(t_c) & p_{12}(t_c) & \cdots & p_{1(n\cdot m)}(t_c) \\ p_{21}(t_c) & p_{22}(t_c) & \cdots & p_{2(n\cdot m)}(t_c) \\ \cdots & \cdots & \cdots & \cdots \\ p_{(n\cdot m)1}(t_c) & p_{(n\cdot m)2}(t_c) & \cdots & p_{(n\cdot m)(n\cdot m)}(t_c) \end{bmatrix}, \quad \begin{matrix} 0 \leq p_{ij}(t_c) \leq 1 \\ \sum_{j=1}^{(n\cdot m)} p_{ij}(t_c) = 1, \quad i = 1, 2, \ldots, (n\cdot m). \end{matrix} \tag{3}$$

$$\boldsymbol{P} = average\left\{\boldsymbol{P}'(t_b), \quad \boldsymbol{P}'(t_{b+1}), \quad \boldsymbol{P}'(t_{b+2}), \quad \ldots, \quad \boldsymbol{P}'(t_{b+e})\right\}, \quad \begin{matrix} t_{b+e} = t_b + e\cdot\Delta t \\ e = 0, 1, 2, 3, \ldots, 199 \end{matrix} \tag{4}$$

The sampling time of the MCM is from 10 s to 15 s (mentioned in the last paragraph of Section 2.2), so the start time t_b for sampling is set as 10 s. According to our previous studies on the parameters of MCM, the model output is not very sensitive to the cell size and time step, if the value is not outrageous. In this study, m and n are separately assigned as 6 and 38, while Δt is set as 0.025 s. In total, there are 200 instantaneous transition probability matrixes which can be obtained during the five-second sampling. With such a condition, the time step should be appropriate to the state divisions. A long time step might make the transition probability matrix more complicated and lead to distorted statistical results, whereas a short time step is not long enough for a particle leaving the current state and moving to the neighboring one.

The state vector transition of a particle between two adjacent time steps or at any time can be described as Equations (5) and (6). During the matrix operations, each component of vector $\boldsymbol{S}(t_c)$ is between 0 and 1, which represents the probability of the particle located at the corresponding state. The probability distribution of the particle state can be easily predicted by these simple matrix operations.

$$\boldsymbol{S}(t_{c+1}) = \boldsymbol{S}(t_c)\boldsymbol{P} \tag{5}$$

$$\boldsymbol{S}(t_{b+e}) = \boldsymbol{S}(t_b)\boldsymbol{P}^e \tag{6}$$

The Monte Carlo cumulative sampling method is used to confirm the certain state of a particle by a random number once the probability distribution of its state is obtained. The random number generated by the computer is limited between 0 and 1. Equation (7) gives the specific algorithm to calculate the state number sn that the particle is marked with at the time t_c according to its state vector $\boldsymbol{S}(t_c)$.

$$\sum_{i=0}^{sn-1} s_i(t_c) < r_0 \leq \sum_{i=0}^{sn} s_i(t_c), \quad \begin{array}{l} r_0 = random(0,1) \\ s_0(t_c) = 0 \ , \quad sn = 1,2,3,\ldots,(n{\cdot}m) \ . \end{array} \tag{7}$$

The state number obtained is equivalent to the cell number in the 2D CFB riser. The approach taken here is to randomly arrange the particles in the cell sn which they are marked with. The whole Markov process of particles uses the CFD-DEM calculated particle information at the time 15 s as the initialization and then calculates the particle movement according to the MCM described above.

3. Results and Discussion

3.1. Computing Efficiency

MCM is initialized by using the CFD-DEM results at 15 s and then continues to simulate by using the stochastic model. It takes about 50 h for the CFD-DEM of the subsequent 5 s simulation, whereas it costs only about 30 min for the MCM. That is, the MCM offers a computational speed that is approximately 100 times faster than that of the CFD-DEM.

3.2. Transition Probability Matrix

The transition probability matrix $\boldsymbol{P}$ is one of the most important factors for the stochastic model and it has the convenience to express some macroscopic properties of the CFB riser.

Figure 3 gives the transition probability matrixes expressed by bar graphs under four fluidized velocities. The transition probability p_{ij} corresponds to the probability under the state number i and the transition number j in the histograms. Figure 3a shows three obvious regions from the left to the right of the graph, where there exist nonzero values in $\boldsymbol{P}$ while the fluidized velocity is 3 m/s. In the first region, the state number i is from 210 to 228, which represents the top area of the CFB riser according to Figure 1, and the transition number j is from 1 to 37, which represents the bottom area of the CFB riser. So, the first nonzero region of $\boldsymbol{P}$ indicates that particles have the certain probability to move from the top to the bottom of the bed. The reason for this kind of particle motion is that the particles are immediately fed into the inlet of bed when they get out of the top of the bed. In the second nonzero region of $\boldsymbol{P}$, the transition number j is around the state number i, and the numerical difference $(i - j)$ varies from -20 to 30 (there are 6 divisions in the width and 38 divisions in the height of the CFB riser for the space state division), which means that the particles have the probability for both vertical and lateral movement at the next time

step from their original positions. The third nonzero region of $\boldsymbol{P}$ is a small area, where the state number i is from 1 to 12, and the transition number is from 214 to 228, which means that the particles have the probability to fall out of the bottom of the bed and then be fed into the outlet of the bed, as the simulated CFB riser is assumed to be an infinite circulating system.

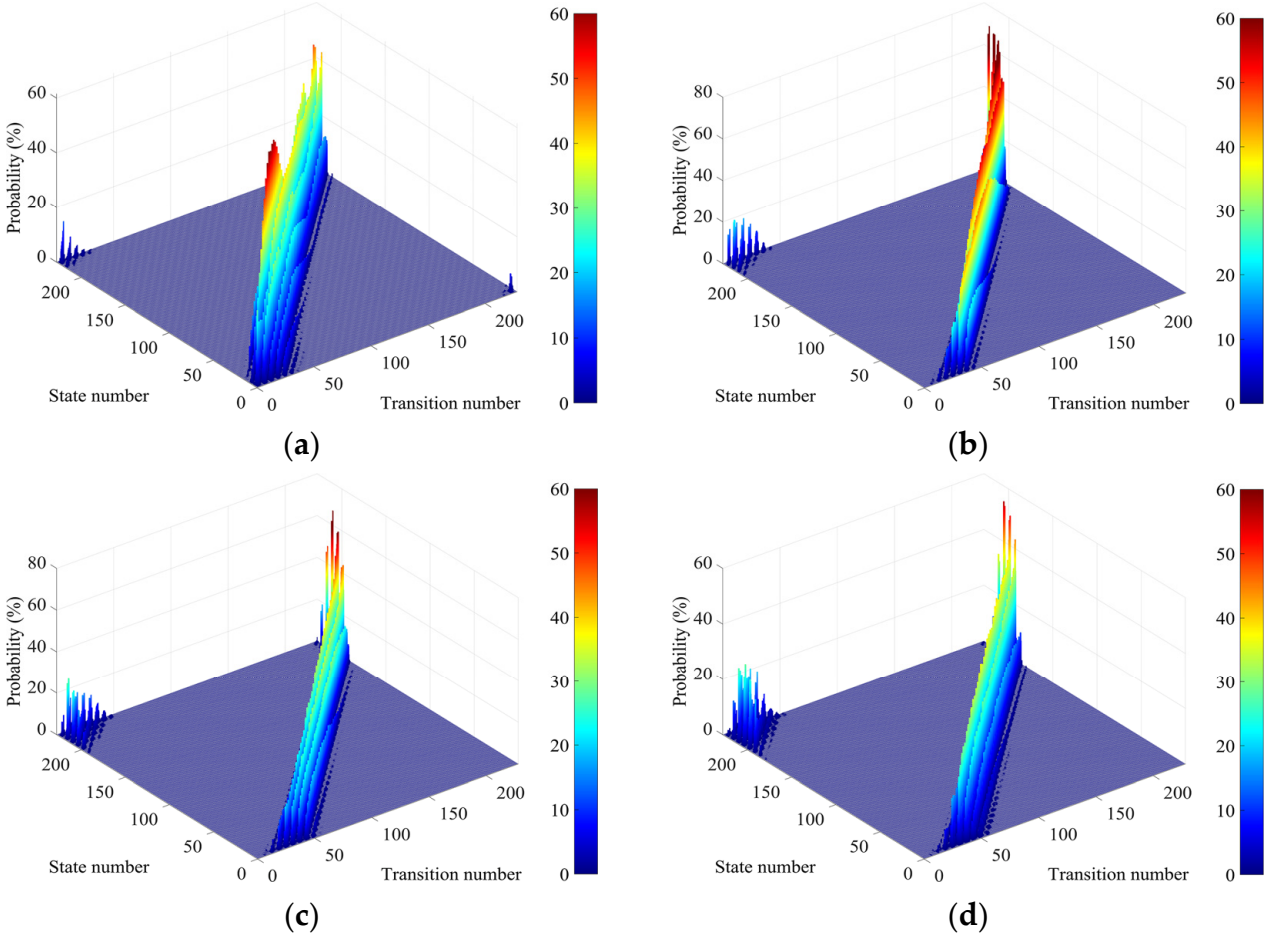


Figure 3. Bar graphs of the transition probability matrixes. Fluidized air velocity: (**a**) 3 m/s; (**b**) 4 m/s; (**c**) 6 m/s; (**d**) 8 m/s.

When the velocity of fluidization rises to 4 m/s or higher, the first nonzero region of $\boldsymbol{P}$ becomes larger, the second nonzero region gradually moves to the area where the state number i is smaller than the transition number j, and the third nonzero region gradually disappears with the increase in the fluidized velocity, as shown in Figure 3b–d. The change in $\boldsymbol{P}$ indicates that the particles prefer to move upward rather than fall.

$$\boldsymbol{S}(t_0) = [\underbrace{1/6, 1/6, \ldots, 1/6}_{s_1 \sim s_6}, \underbrace{0, 0, \ldots, 0}_{s_7 \sim s_{228}}] \tag{8}$$

It is easy to calculate the probability distribution of the particle positions by using Equations (5) and (6) once $\boldsymbol{P}$ and $\boldsymbol{S}$ are obtained. Figure 4 shows the probability distribution for the particle positions at 0.25 s, 0.5 s, and 0.75 s under the fluidized velocity of 3 m/s after a batch of particles are fed into the inlet of the CFB riser. The initial state vector $\boldsymbol{S}(t_0)$ is shown as Equation (8), which expresses that a batch of particles are uniformly fed into the inlet of bed.

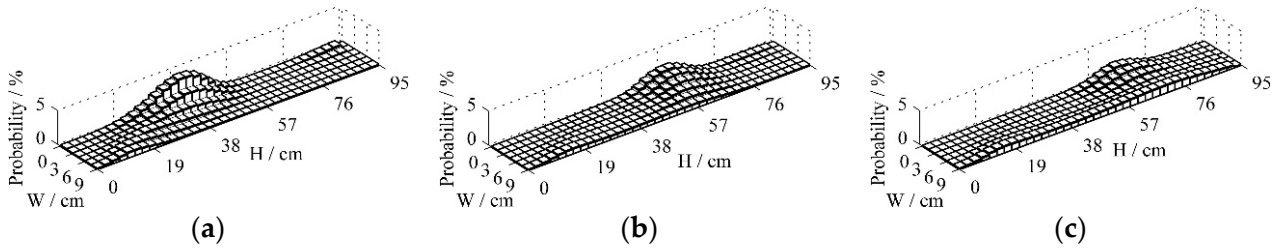


Figure 4. Probability distribution for the positions of a batch of particles after being put into the inlet of the CFB riser. Fluidization velocity of 3 m/s at time (**a**) 0.25 s; (**b**) 0.5 s; and (**c**) 0.75 s.

The probability that particles appear in the upper-left corner of the bed in Figure 4a indicates that some particles fall out of the bottom of the bed and are put into the top of the bed at the time 0.25 s, which indicates the particle backflow at lower velocities and agrees with the analysis of the transition probability $\boldsymbol{P}$ in Figure 3a. Figure 4a also shows that most particles prefer to move upward on one side of the bed, whereas particles on the other side of the bed move upward at a much slower rate and even seem to have a downward trend (particle backflow) combined with Figure 4b,c. The result is consistent with the motion characteristics of particle clusters under low fluidized air velocity. Figure 4c indicates that most particles do not get out of the bed within 0.75 s.

Figure 5 gives the probability distribution of the particle positions at 0.05 s, 0.1 s, and 0.15 s under the fluidized velocity of 4 m/s. The nonzero probability area is clearly much more concentrated than that shown in Figure 4, indicating that almost all particles flow upward and gather in a small area. None of the particles get out of the bed within 0.15 s and the particle backflow is invisible.

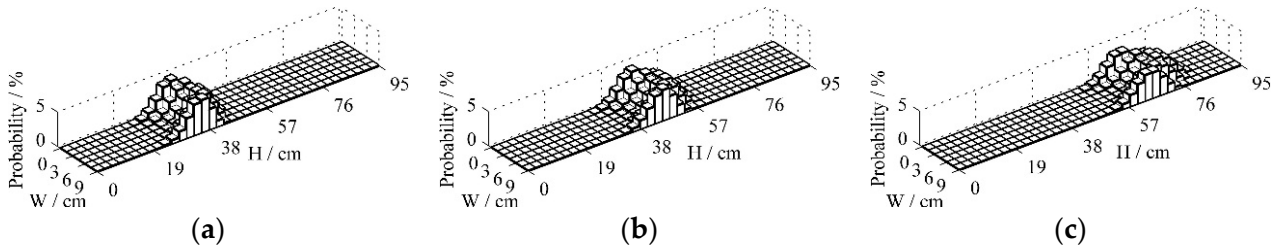


Figure 5. Probability distribution for the positions of a batch of particles after being put into the inlet of the CFB riser. Fluidization velocity of 4 m/s at time (**a**) 0.05 s; (**b**) 0.1 s; and (**c**) 0.15 s.

Figure 6 gives the probability distribution of the particle positions at 0.05 s, 0.1 s, and 0.15 s under the fluidized velocity of 6 m/s. With the increase in the fluidized velocity, the particle rising velocity increases, and particles gradually spread in the vertical direction. There are few particles getting out of the bed within 0.15 s.

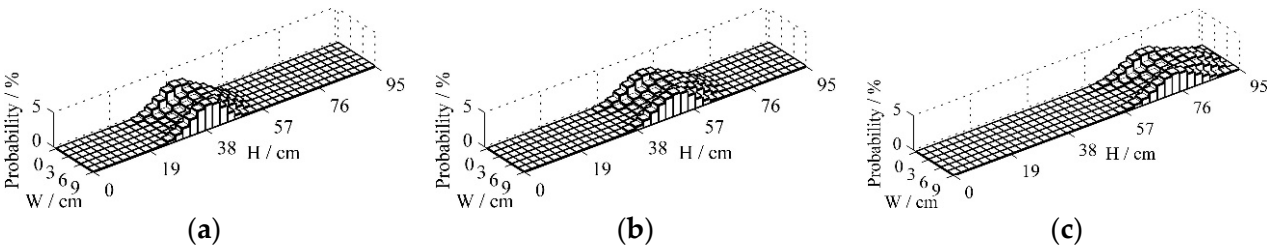


Figure 6. Probability distribution for the positions of a batch of particles after being put into the inlet of the CFB riser. Fluidization velocity of 6 m/s at time (**a**) 0.05 s; (**b**) 0.1 s; and (**c**) 0.15 s.

Figure 7 gives the probability distribution of the particle positions at 0.05 s, 0.1 s, and 0.15 s under the fluidized velocity of 8 m/s. Particles in the middle of the bed clearly flow

upward at a faster rate than those on both sides of the bed, which is consistent with the motion characteristics of particle clusters under high fluidized air velocity. Some of the particles get out of the bed at the time 0.15 s, which indicates that the averaged particle residence time of CFB reduces with the increase in the fluidized velocity.

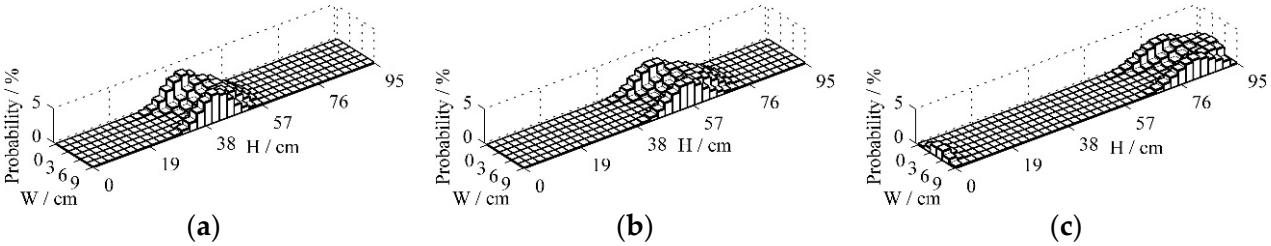


Figure 7. Probability distribution for the positions of a batch of particles after being put into the inlet of the CFB riser. Fluidization velocity of 8 m/s at time (**a**) 0.05 s; (**b**) 0.1 s; and (**c**) 0.15 s.

3.3. Residence Time Distribution

Figure 8 gives the particle residence time distribution (RTD) calculated by two models. The E(RT) is used to represent the mathematical expectation of the particle residence time, which means the averaged value. The SD(RT) represents the degree of variation in particle residence times, indicating how dispersed the values are. Obviously, the fluidized velocity increasing leads to a decrease in the E(RT). The CFD-DEM simulated profile of the RTD shown in Figure 8a displays distinct multiple peaks and the RTD spans a much broader range compared to the RTDs depicted in Figure 8b–d. As the fluidized bed velocity increases, the SD(RT) decreases.

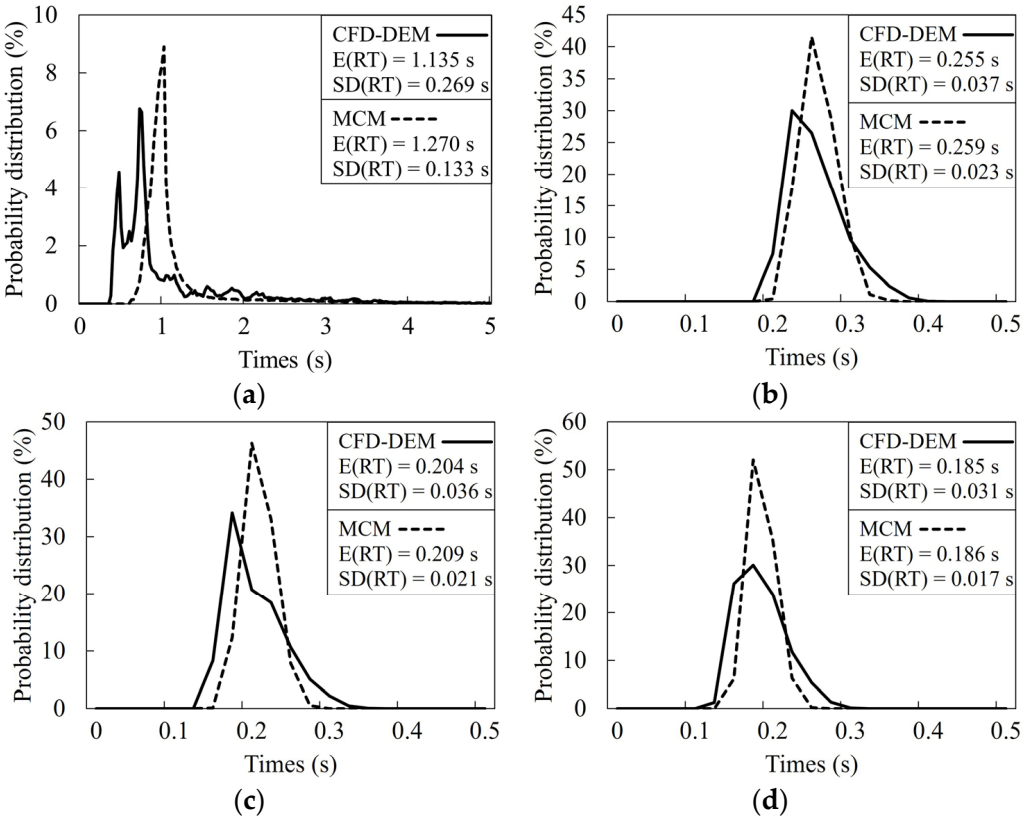


Figure 8. Particle RTD calculated by two models. Fluidization velocity: (**a**) 3 m/s; (**b**) 4 m/s; (**c**) 6 m/s; (**d**) 8 m/s.

Additionally, the SD(RT) shown in Figure 8a is significantly greater than that in the other three figures. Comparing the results suggests that, when the fluidized velocity reaches 3 m/s, a significant number of particles may be falling back in the CFB riser, which is indicative of the typical annular-core flow structure. As the fluidized bed air velocity rises to 4 m/s or higher, the occurrence of particle backflow diminishes, with a more concentrated RTD and a smaller SD(RT).

In comparison to the CFD-DEM results, the simulated RTDs of particles for the MCM are noticeably more condensed around the E(RT)s across all four fluidized velocities, as shown in Figure 8. Table 2 provides a detailed comparison of E(RT) and SD(RT) between the MCM and CFD-DEM. The PD represents the percentage difference between the results obtained from the CFD-DEM and MCM. The quantitative comparison of the SD(RT) suggests that the MCM-simulated RTD tends to emphasize the primary particle residence time more prominently. Meanwhile, it disregards the secondary range of particle residence times. The MCM-simulated RTD exhibits a notably smaller SD(RT) in comparison to the CFD-DEM results. At fluidization velocities of 4 m/s, 6 m/s, and 8 m/s, the difference in simulated particle E(RT)s between the MCM and the CFD-DEM is less than 3%. However, when the fluidization velocity is reduced to 3 m/s, the difference in the E(RT) between the two models increases to approximately 12%. The reason is low fluidization velocity can lead to significant cluster backflow, which causes more dispersed RTD, and the time-averaged $\boldsymbol{P}$ used in MCM cannot reflect this change.

Table 2. RTD comparison between two models.

U, m/s	PD of E(RT), %	PD of SD(RT), %	MD of RTD, %	R^2
3	11.89	−50.55	0.0185	0.32
4	1.57	−37.84	0.238	0.78
6	2.45	−41.67	0.380	0.51
8	0.54	−45.16	0.328	0.71

The Minkowski distances (MDs) for the simulated RTDs are calculated to demonstrate the similarity between two model results as shown in Equation (9), which can quantify the closeness of two arrays (E and F) in terms of both numerical values and distributions. The coefficient of determination (R^2) can be used to indicate the degree of fit between the simulation results of a statistical model and the sample data. The maximum value of R^2 is 1. The closer the value of R^2 is to 1, the better the fit of the simulation results to the sample data. Conversely, a smaller value of R^2 indicates a poorer fit of the simulation results to the sample data. The calculation method for R^2 is shown in Equation (10). Where O_i represents the simulation results, P_i represents the sample data, and n represents the amount of data. For simulation results like RTD, which mainly reflect the time-averaged characteristics of the data, R^2 can objectively represent the degree of fit to the sample data.

As indicated in Table 2, at the fluidized velocity of 3 m/s, the MD value remains low, despite a notable discrepancy in the distribution of the simulated RTD of two models at a particle residence time close to 0.05 s. As the fluidized velocity increases, the MD value also increases, which indicates that the simulated RTDs of the MCM have a clear difference with the CFD-DEM on the whole distribution patterns. The R^2 value indicates a weak correlation between the RTD simulated by the MCM and that simulated by CFD-DEM, suggesting that the MCM can simulate the macroscopic particle motion under the guidance of the transition probability matrix, rather than being a simple reproduction of the CFD-DEM simulation results.

$$\mathrm{MD}_{EF} = \sqrt[k]{\sum_{j=1}^{n} |e_j - f_j|^k} \tag{9}$$

$$R^2 = \frac{\left[\sum_{i=1}^{n} (O_i - \overline{O_i}) \cdot (P_i - \overline{P_i})\right]^2}{\sum_{i=1}^{n} (O_i - \overline{O_i}) \cdot \sum_{i=1}^{n} (P_i - \overline{P_i})} \tag{10}$$

3.4. Particle Distribution

Figure 9a gives the simulated particle distribution snapshots of the CFD-DEM from 15 s to 15.7 s, while the fluidized velocity is 4 m/s. Particles are assigned two distinct colors at the 15 s mark. Particles located at the height of 30 cm to 60 cm within the bed are marked as purple, and others are marked as green. In this way, the particle flow structure and mixing process can be clearly obtained. The formation of particle clusters and annular-core flow structure is evident in Figure 9a, and over time, the particles with different initial heights within the bed gradually blend, as indicated by the distribution of colors. The purple particles exhibit a trend of faster upward movement in the middle and slower upward movement on both sides. Additionally, the purple particles maintain a band-like distribution characteristic before 15.3 s, indicating that the radial mixing speed of the particles within the bed is relatively slow.

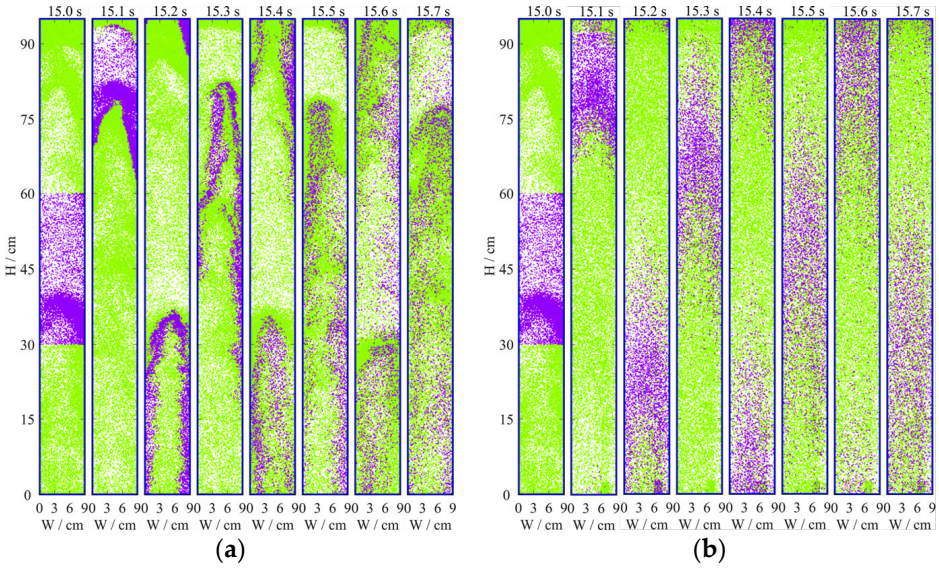


Figure 9. Particle distribution comparison of the two models. Fluidization velocity: 4 m/s. (**a**) CFD-DEM; (**b**) MCM.

The MCM-simulated particle mixing is shown in Figure 9b at the same period and under the same fluidized velocity. A notable feature is that the clusters of particles are barely noticeable. From the distribution trend of purple particles within the bed, the overall trend of annular-core flow structure of particles can be clearly observed, and the radial diffusion of the banded purple particles is faster than the results predicted by the CFD-DEM simulation. The reason for this result is that MCM belongs to the statistical modeling category and simulates based on the time-averaged transition probability matrix. Therefore, it is difficult for MCM to reproduce the instantaneous motion characteristics of particles in the sample. However, the macroscopic particle motion law of time uniformity can be well presented.

3.5. Particle Mixing

For a deeper analysis of MCM-simulated particle mixing, Figure 10 provides a comprehensive comparison of axial particle mixing among two models, across four different fluidized velocities. The curves in the figure represent the proportion of particles that were in the lower half of the bed at the 15 s mark and that remain in the lower half over time (as a percentage of the total number of particles in the bed), which can indicate the axial particle mixing trend within the bed.

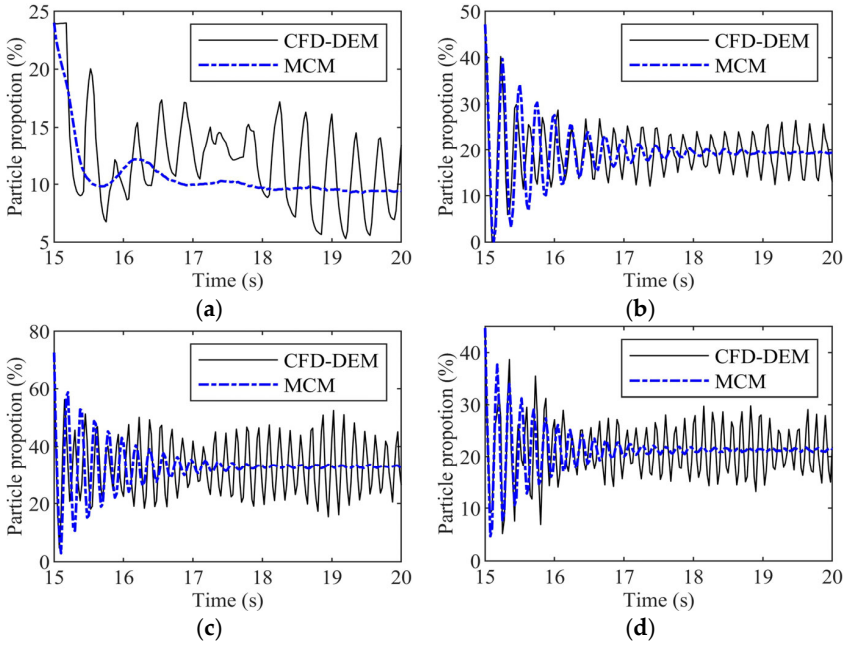


Figure 10. Axial particle mixing of two models. Fluidization velocity: (**a**) 3 m/s; (**b**) 4 m/s; (**c**) 6 m/s; (**d**) 8 m/s.

At the fluidized velocity of 3 m/s, Figure 10a illustrates that approximately 24% of the total particles are present in the lower half of the bed at the 15 s. The two models exhibit a similar overall macro-mixing trend, with roughly half of the particles shifting to the upper half of the bed after 5 s of simulation. The mixing curve of the MCM appears much more smoothly, in contrast to the CFD-DEM simulated mixing curves which exhibit frequent and abrupt fluctuations. This may be attributed to the fact that the MCM does not capture the recurrence of particle clusters.

As depicted in Figure 10b, at the fluidized velocity of 4 m/s, approximately 47% of the total particles are in the lower half of the bed at the 15s time point. The two models both demonstrate good axial mixing of particles within the subsequent 5 s of the simulation. Before 17 s, the MCM-simulated mixing curve exhibits instantaneous fluctuations with amplitudes and frequencies approximately like those from CFD-DEM simulation results. However, after 17 s, the curve from the MCM simulation tends to smooth out, and closely aligns with the time-averaged mixing value of the CFD-DEM. In contrast, the mixing curve from the CFD-DEM simulation continues to exhibit instantaneous fluctuations with a certain amplitude and frequency. The reason is the formation and variation in particle clusters simulated by CFD-DEM lead to a transient inhomogeneity in the particle distribution within the bed. Similar particle mixing of the two models at fluidized velocities of 6 and 8 m/s is illustrated in Figure 10c,d. Additionally, there is a noticeable increase in the axial mixing speed and fluctuation frequency of particles as the fluidized velocity increases.

Based on the above analysis, the MCM can simulate the overall trend of particle motion well. When it comes to detailed instantaneous particle structure (such as par-

ticle clusters) and motion characteristics, the MCM needs to be further improved for practical applications.

4. Conclusions

The MCM is developed to simulate the particle dynamics within a 2D CFB riser sampling from CFD-DEM results. The MCM has the advantages of high computing speed and low computational load when compared to the CFD-DEM. In addition, the MCM has the convenience to describe the macroscopic particle movement characteristics by the transition probability matrix, which agrees well with the statistical samples. However, the MCM-simulated particle movement, RTD, and particle mixing represent time-averaged characteristics, instead of instantaneous characteristics. It is hard for the MCM to simulate the structures of particle clusters. Thus, an extra cluster model may be established to introduce the instantaneous effect on the particle moment by clusters for the MCM. In addition, more statistical samples from elaborate experiments are needed to support the MCM. Based on the above analysis, the MCM is not a full replacement for the CFD-DEM for now, but rather a complementary approach for cases where computational efficiency and a macroscopic particle movement trend are critical. The establishment of the MCM, with a combination of mass transfer, heat transfer, and chemical reaction sub-models, will be a promising method for efficient simulation of industrial dense gas–solid flows in the future. The modeling process and calculation results of MCM do not include information on gas-phase flow. Coupling MCM with gas-phase flow is a primary issue to be addressed in the subsequent development of reaction models. As the MCM does not solve fundamental mechanical equations, resulting in high computational speed, the simulation of gas-phase flow in statistical models should also not solve the basic equations of CFD. Classical gas–solid two-phase models provide specific simplified descriptions of gas-phase flow in both dense and dilute phases. By referring to the establishment process of the MCM, the description of the gas phase in two-phase models can complement the particle phase information provided by statistical models. Therefore, coupling the MCM with traditional two-phase models is a potential approach to address the gas-phase flow issues in statistical models. Further heat and mass transfer research on the MCM can be based on the gas–solid MCM mentioned above.

Funding: This research was supported by the Suqian University Research Launch Project (grant no. 2022XRC099), Suqian Key Laboratory of Intelligent Manufacturing (grant no. M202108), and the Jiangsu Engineering Research Center of Key Technology for Intelligent Manufacturing Equipment.

Data Availability Statement: The data presented in this study are available in the article. Further inquiries can be directed to the corresponding author.

Conflicts of Interest: The authors declare no conflicts of interest.

Nomenclature

H	CFB riser height (cm)
p_{ij}	transition probability from state s_i to state s_j
$\boldsymbol{P'}$	instantaneous transition probability matrix
$\boldsymbol{P}$	average transition probability matrix
s	space state of MCM
$\boldsymbol{S}$	state vector of MCM
Δt	MCM time step (s)
U	fluidization velocity (m/s)
W	CFB riser width (cm)

References

1. Chao, C.; Deng, Y.; Dewil, R.; Baeyens, J.; Fan, X. Post-combustion carbon capture. *Renew. Sustain. Energy Rev.* **2021**, *138*, 110490. [CrossRef]
2. Wang, J.W. Continuum theory for dense gas-solid flow: A state-of-the-art review. *Chem. Eng. Sci.* **2020**, *215*, 115428. [CrossRef]
3. Li, Y.K.; Guo, T.; Guo, X.T.; Hu, X.D.; Guo, Q.J.; He, S.Z.; Zhou, Z.M. Computational particle fluid dynamics simulation of gas-solid flow in a 3 MW th dual-circulation fluidized bed for chemical looping process. *Carbon. Resour. Convers.* **2024**, *7*, 100232. [CrossRef]
4. Haghgoo, M.R.; Bergstrom, D.J.; Spiteri, R.J. Identifying particle flow structures in a dense gas-particle fluidized bed. *Int. J. Heat Fluid Flow* **2024**, *108*, 109495. [CrossRef]
5. Zarepour, M.; Bergstrom, D.J.; Zhang, L.F.; Spiteri, R.J. The effect of collision parameters on the 3D Eulerian simulation of a thin rectangular bubbling fluidized bed. *Int. J. Heat Fluid Flow* **2024**, *107*, 109354. [CrossRef]
6. Li, X.F.; Xu, Q.L.; Wang, S.; Luo, K.; Fan, J.R. A novel data-driven reduced-order model for the fast prediction of gas-solid heat transfer in fluidized beds. *Appl. Therm. Eng.* **2024**, *253*, 123670. [CrossRef]
7. Lian, G.Q.; Zhong, W.Q. Coupling CFD-DEM with cohesive force and chemical reaction sub-models for biomass combustion in a fluidized bed. *Fuel* **2023**, *350*, 128858. [CrossRef]
8. Yu, J.H.; Wang, S.; Luo, K.; Fan, J.R. CFD-DEM modeling of dense gas-solid reacting flow in the framework of GPU. *Chem. Eng. J.* **2024**, *484*, 149480. [CrossRef]
9. Li, H.; Liu, D.Y.; Ma, J.L.; Chen, X.P. Simulation of a Wurster fluidized bed by CFD-DEM with a cohesive contact model. *Chem. Eng. Res. Des.* **2022**, *177*, 157–166. [CrossRef]
10. Xu, D.; Wang, S.; Shen, Y.S. An improved CFD-DEM modelling of raceway dynamics and coke combustion in an industrial-scale blast furnace. *Chem. Eng. J.* **2023**, *455*, 140677. [CrossRef]
11. Ma, H.Q.; Zhou, L.Y.; Liu, Z.H.; Chen, M.Y.; Xia, X.H.; Zhao, Y.Z. A review of recent development for the CFD-DEM investigations of non-spherical particles. *Powder Technol.* **2022**, *412*, 117972. [CrossRef]
12. Wang, S.; Shen, Y.S. Coarse-grained CFD-DEM modelling of dense gas-solid reacting flow. *Int. J. Heat Mass. Transf.* **2022**, *184*, 122302. [CrossRef]
13. Hoffmann, A.; Dehling, H. A Stochastic modelling approach to particle residence time distribution in continuous fluidized beds. In Proceedings of the Third World Congress on Particle Technology, Brighton, UK, 6–9 July 1998; pp. 258–270.
14. Dehling, H.G.; Hoffmann, A.C.; Stuut, H.W. Stochastic models for transport in a fluidized bed. *SIAM J. Appl. Math.* **1999**, *60*, 337–358. [CrossRef]
15. Dehling, H.G.; Dechsiri, C.; Gottschalk, T.; Wright, P.C.; Hoffmann, A.C. A stochastic model for mixing and segregation in slugging fluidized beds. *Powder Technol.* **2007**, *171*, 118–125. [CrossRef]
16. Berthiaux, H.; Mizonov, V. Applications of Markov chains in particulate process engineering: A review. *Can. J. Chem. Eng.* **2004**, *82*, 1143–1168. [CrossRef]
17. Ammarcha, C.; Gatumel, C.; Dirion, J.L.; Cabassud, M.; Mizonov, V.; Berthiaux, H. Powder flow and mixing in a continuous mixer operating in either transitory or steady-state regimes: Mesoscopic Markov chain models. *Powder Technol.* **2019**, *346*, 116–136. [CrossRef]
18. Doucet, J.; Hudon, N.; Bertrand, F.; Chaouki, J. Modeling of the mixing of monodisperse particles using a stationary DEM-based Markov process. *Comput. Chem. Eng.* **2008**, *32*, 1334–1341. [CrossRef]
19. Ponomarev, D.; Mizonov, V.; Gatumel, C.; Berthiaux, H.; Barantseva, E. Markov-chain modelling and experimental investigation of powder-mixing kinetics in static revolving mixers. *Chem. Eng. Process.* **2009**, *48*, 828–836. [CrossRef]
20. Ponomarev, D.; Mizonov, V.; Berthiaux, H.; Gatumel, C.; Gyenis, J.; Barantseva, E. A 2D Markov chain for modelling powder mixing in alternately revolving static mixers of Sysmix® type. *Chem. Eng. Process.* **2009**, *48*, 1495–1505. [CrossRef]
21. Gottschalk, T.; Dehling, H.G.; Hoffmann, A.C. Multiphase stochastic model for fluidized beds. *Phys. Rev. E* **2008**, *77*, 031306. [CrossRef]
22. Catak, M.; Cronin, K.; Medina-Tellez, D. Markov Chain Modeling of Fluidized Bed Granulation Incorporating Simultaneous Aggregation and Breakage. *Ind. Eng. Chem. Res.* **2011**, *50*, 10811–10823. [CrossRef]
23. Catak, M.; Bas, N.; Cronin, K.; Tellez-Medina, D.; Byrne, E.P.; Fitzpatrick, J.J. Markov chain modelling of fluidised bed granulation. *Chem. Eng. J.* **2010**, *164*, 403–409. [CrossRef]
24. Mizonov, V.; Mitrofanov, A.; Ogurtzov, A.; Tannous, K. Modeling of Particle Concentration Distribution in a Fluidized Bed by Means of the Theory of Markov Chains. *Part. Sci. Technol.* **2014**, *32*, 171–178. [CrossRef]
25. Mitrofanov, A.; Mizonov, V.; Tannous, K.; Ovchinnikov, L. A Markov chain model to describe fluidization of particles with time-varying properties. *Part. Sci. Technol.* **2018**, *36*, 244–253. [CrossRef]
26. Mitrofanov, A.; Mizonov, V.; Camelo, A.; Tannous, K. Application of the theory of Markov chains to theoretical study of processes in a circulating fluidized bed. *Part. Sci. Technol.* **2019**, *37*, 1028–1033. [CrossRef]

27. Harris, A.T.; Thorpe, R.B.; Davidson, J.F. Stochastic modelling of the particle residence time distribution in circulating fluidised bed risers. *Chem. Eng. Sci.* **2002**, *57*, 4779–4796. [CrossRef]
28. Tjakra, J.D.; Bao, J.; Hudon, N.; Yang, R.Y. Modeling collective dynamics of particulate systems under time-varying operating conditions based on Markov chains. *Adv. Powder Technol.* **2013**, *24*, 451–458. [CrossRef]
29. Bouffard, J.; Bertrand, F.; Chaouki, J. A multiscale model for the simulation of granulation in rotor-based equipment. *Chem. Eng. Sci.* **2012**, *81*, 106–117. [CrossRef]
30. Alobaid, F.; Almohammed, N.; Farid, M.M.; May, J.; Rossger, P.; Richter, A.; Epple, B. Progress in CFD Simulations of Fluidized Beds for Chemical and Energy Process Engineering. *Prog. Energy Combust. Sci.* **2022**, *91*, 100930. [CrossRef]

Disclaimer/Publisher's Note: The statements, opinions and data contained in all publications are solely those of the individual author(s) and contributor(s) and not of MDPI and/or the editor(s). MDPI and/or the editor(s) disclaim responsibility for any injury to people or property resulting from any ideas, methods, instructions or products referred to in the content.